Supporting Information

Peschek et al. 10.1073/pnas.1308898110

SI Materials and Methods

Quaternary Structure Analysis. Size exclusion chromatography (SEC) of αB-crystallin (αB)-WT and its phosphorylation-mimicking mutants was performed using a TSK 4000 PW column (Tosoh) equilibrated in PBS.

Analytical ultracentrifugation (AUC) was carried out using a ProteomeLab XL-A (Beckman-Coulter) equipped with absorbance optics. All experiments were performed in PBS at 20 °C. For the determination of the quaternary structure of all αB variants, sedimentation velocity (SV) experiments were performed with protein concentrations of 30 μM at a rotor speed of 30,000 rpm using an An-50 Ti rotor (Beckman Coulter). Data analysis was carried out either according to the dc/dt method (1) using the DCDT+ software (2) or the c(s) method with time invariant (TI) and radial invariant (RI) noise fitting using the SEDFIT software (3). For the detection of labeled protein, a fluorescence detection system (Aviv) was used.

Sedimentation equilibrium (SE) experiments were performed with 5 μM αB at 12,000 rpm using an An-50 Ti rotor (Beckman Coulter). Data were fitted to a exponential single component model as described by Eq. **S1**

$$c(r) = c_0 \cdot e^{\frac{M\left(1-\bar{V}\rho\right)\omega^2\left(r^2-r_0^2\right)}{2RT}}. \qquad [S1]$$

Image Processing. For image processing, cryo-electron microscopy (cryo-EM) micrographs of αB-3E were selected by their power spectra (13 in total) and digitized at a step size of 8.47 μm, resulting in a calibrated pixel size of 1.71 Å at the specimen level. Well-separated particle images were semiautomatically selected and extracted into boxes using "Boxer" from the EMAN software package (4). CTFIT, also from the EMAN software package, was used to determine the defocus and to correct the phase contrast transfer function by phase flipping. The defocus values of the micrographs ranged between 0.9 and 1.8 μm. All further image processing procedures and the 3D reconstruction were carried out within the IMAGIC suite (5).

For a preliminary reference-free analysis of the αB-3E cryo-EM data, 24,424 single particle projection images were translationally aligned with respect to their individual centers of mass and subjected to an initial multivariate statistical analysis (MSA). The first three eigenimages (statistical difference images) indicated substantial size variations and were thus used to classify the data into four size-related subpopulations by MSA. Class averages of individual subpopulations were obtained in a next MSA without any further alignment and using the first 20 eigenimages for classification. As these class averages strongly resembled projections of 3D models of αB oligomers obtained in a previous cryo-EM study (6), the data were further separated by projection matching cycles using pseudoatomic models of αB oligomers as initial references.

As estimated from the Fourier shell correlation curve using the FSC-0.5 cutoff criterion (7), the resolutions of the reconstructed αB-3E 24-, 12-, and 6-mers are 17.5, 16, and 14 Å, respectively, whereas the resolutions of their αB-WT counterparts are 9.5, 11.5, and 18 Å.

For a detailed heterogeneity/variance analysis of the models of hexameric assemblies, 100 3D asymmetric reconstructions of 15 randomly selected class averages (500 in total) from the 6-mer data set were generated. The Euler angles of the centered class averages were assigned by multireference alignment (MRA) where 2D projections obtained from the symmetric 6-mer model (Fig. 2*A*) served as references. All resulting random 3D reconstructions were then subjected to 3D MSA followed by 3D classification into 10 classes (8). Independent validation was performed by independent random reconstruction parameters and cycles and finally by the correlation between input class averages and 3D reprojections of the calculated models.

Phosphorylation of αB. αB was phosphorylated in vitro by incubation with mitogen-activated protein kinase-activated protein (MAPKAP) kinase 2 (Millipore). The reaction was performed at 30 °C in 50 mM Tris·HCl/pH 7.5, 10 mM $MgCl_2$, 0.1 mM EDTA, 2 mM DTT, and 0.01% Brij 35 for 48 h. The reaction mixture contained 50 μM αB, 0.5 μg/mL of the kinase, and 1 mM ATP. Phosphorylation was confirmed by electrophoresis using 12.5% (wt/vol) Phos-tag acrylamide gels (Wako Pure Chemicals Industries).

LC-MS. For the identification by LC-MS of the cleavage products from limited proteolysis, samples were applied to a reverse-phase C4 column (Thermo Scientific) and were eluted with a water to an acetonitrile (ACN) gradient (with 0.1% formic acid) online into the MS. Spectra were recorded from 500 to 2,000 *m/z* on a LTQ FT Ultra (Thermo Scientific) with a resolution of 100,000@400 *m/z*. The protein-containing spectra were averaged and deconvoluted using ProMass 2.8 (Thermo Scientific) with default settings for large proteins and were matched to an in silico digest of αB variants using Biotools software (Bruker).

Preparation of HeLa Lysates. HeLa cells were grown at 37 °C with 5% CO_2 in RPMI (Invitrogen) supplemented with 10% FCS (Invitrogen). Cells were trypsinized at a confluency of ∼90%. After centrifugation (4 min, 500 × *g* at 4 °C), the supernatant was removed, and the cells were resuspended in cold hypotonic buffer (40 mM sodium phosphate, pH 7.4) in the presence of protease inhibitor Mix M (Serva). The HeLa cell suspension was incubated for 15 min on ice to allow for hypotonic swelling. To disrupt the cells, the suspension was passed several times through a sterile needle (Neolus with 6 mm diameter; Terumo Europe). The lysate was cleared by centrifugation (10 min at 12,000 × *g*, 4 °C), the supernatant was decanted into sterile tubes, and 10× PBS stock was added to yield physiological salt concentrations. The lysate was ATP depleted by addition of hexokinase (10 U/mL) in the presence of 2 mM $MgSO_4$ for 30 min at 10 °C. The cleared and ATP-depleted HeLa cell lysate was frozen in liquid nitrogen and stored at −80 °C.

Identification of Aggregated HeLa Lysate Proteins by MS. Coomassie-stained lanes were sliced into six parts and treated as individual samples. Proteins were reduced, alkylated, and digested overnight with trypsin (9). Peptides were extracted in five steps by adding sequentially 50 μL of buffer A (water with 0.1% formic acid), ACN, buffer A, ACN, and ACN. After each step, samples were treated for 15 min by sonication. After steps 2, 4, and 5, the supernatant was removed from the gel slices and collected for further processing.

The collected supernatants were pooled, concentrated in a speed vac (DNA120; Thermo Scientific) to ∼20 μL final volume, and filtered through a 0.22-μm centrifuge filter (Millipore). Peptides were loaded onto an Acclaim PepMap RSLC C18 trap column (Thermo Scientific) with 5 μL/min and separated on a PepMap RSLC C18 column (75 μm × 150 mm, C18, 2 μm, 100 A; Thermo Scientific) at a flow rate of 0.2 μL/min. A linear gradient from 5% to 35% buffer B (100% ACN with 0.1% formic acid) eluted the peptides in 60 min to a LTQ Orbitrap XL

(Thermo Scientific). Full scans and six dependent MS^2 scans (collision-induced dissociation, 35% normalized collisional energy; activation Q: 0.25; activation time: 30 ns) were recorded in each cycle.

The MS data derived from the each gel slice were searched against a human proteome reference database containing 71,176 proteins downloaded from the UniProt database (07/17/2012) using the SEQUEST algorithm implemented into the software Proteome Discoverer 1.3 (Thermo Scientific). The search was limited to tryptic peptides containing a maximum of three missed cleavage sites, monoisotopic precursor ions, and a peptide tolerance of 10 ppm for precursors and 0.1 Da for fragment masses. Proteins were identified with two unique peptides with a target false discovery rate for peptides <1% according to the decoy search.

EMSA. EMSA was used to study the binding of p53 to DNA. Cy5-labeled p21-DNA, unspecific DNA of the same length, and p53 (reaction mix) were incubated in DNA binding buffer (80 mM Hepes, pH 8, 15% glycerol, 100 mM KCl, 20 mM $MgCl_2$, 10 mM DTT, 2 mg/mL BSA, and 0.2% TritonX-100) for 15 min. After addition of the reaction mix, the samples were loaded on a 4% polyacrylamide gel. Electrophoresis was carried out in 30 mM Tris, pH 8, 30 mM boric acid, 5 mM EDTA, and 0.1% TritonX-100 for 3 h at 4 °C applying 25 mA per gel. The fluorescence of the Cy5-labeled p21-DNA was detected in a Typhoon 9600 phosphoimager (Amersham).

Hydrodynamic Simulations. Hydrodynamic parameters, e.g., gyration radii and sedimentation coefficients, of αB-3E oligomers were estimated by hydrodynamic simulations conducted within the software package HYDROMIC (10) using 3D reconstructions of 6- and 12-mers as input and the software package HYDROPRO (11) using the volume occupied by a 24-mer and dimers in the pseudoatomic model of αB 24-mer (PDB 2YGD) as input (6).

1. Stafford WF, 3rd (1992) Boundary analysis in sedimentation transport experiments: A procedure for obtaining sedimentation coefficient distributions using the time derivative of the concentration profile. *Anal Biochem* 203(2): 295–301.
2. Philo JS (2006) Improved methods for fitting sedimentation coefficient distributions derived by time-derivative techniques. *Anal Biochem* 354(2):238–246.
3. Schuck P (2000) Size-distribution analysis of macromolecules by sedimentation velocity ultracentrifugation and lamm equation modeling. *Biophys J* 78(3): 1606–1619.
4. Ludtke SJ, Baldwin PR, Chiu W (1999) EMAN: Semiautomated software for high-resolution single-particle reconstructions. *J Struct Biol* 128(1):82–97.
5. van Heel M, Harauz G, Orlova EV, Schmidt R, Schatz M (1996) A new generation of the IMAGIC image processing system. *J Struct Biol* 116(1):17–24.
6. Braun N, et al. (2011) Multiple molecular architectures of the eye lens chaperone αB-crystallin elucidated by a triple hybrid approach. *Proc Natl Acad Sci USA* 108(51):20491–20496.
7. Saxton WO, Baumeister W (1982) The correlation averaging of a regularly arranged bacterial cell envelope protein. *J Microsc* 127(Pt 2):127–138.
8. Simonetti A, et al. (2008) Structure of the 30S translation initiation complex. *Nature* 455(7211):416–420.
9. Haslbeck M, et al. (2004) Hsp42 is the general small heat shock protein in the cytosol of Saccharomyces cerevisiae. *EMBO J* 23(3):638–649.
10. García de la Torre J, Llorca O, Carrascosa JL, Valpuesta JM (2001) HYDROMIC: Prediction of hydrodynamic properties of rigid macromolecular structures obtained from electron microscopy images. *Eur Biophys J* 30(6):457–462.
11. García De La Torre J, Huertas ML, Carrasco B (2000) Calculation of hydrodynamic properties of globular proteins from their atomic-level structure. *Biophys J* 78(2):719–730.

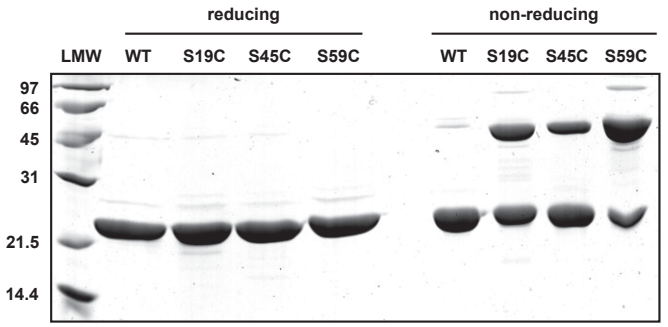

Fig. S1. Proximity of the major phosphorylation sites within the αB-crystallin oligomer. SDS/PAGE analysis of Ser-to-Cys mutants of αB at the phosphorylation sites 19, 45, and 59 on cysteine cross-linking. Although only the monomer bands were detected under reducing conditions, all three Cys mutants showed an additional dimer band in the absence of reducing agent.

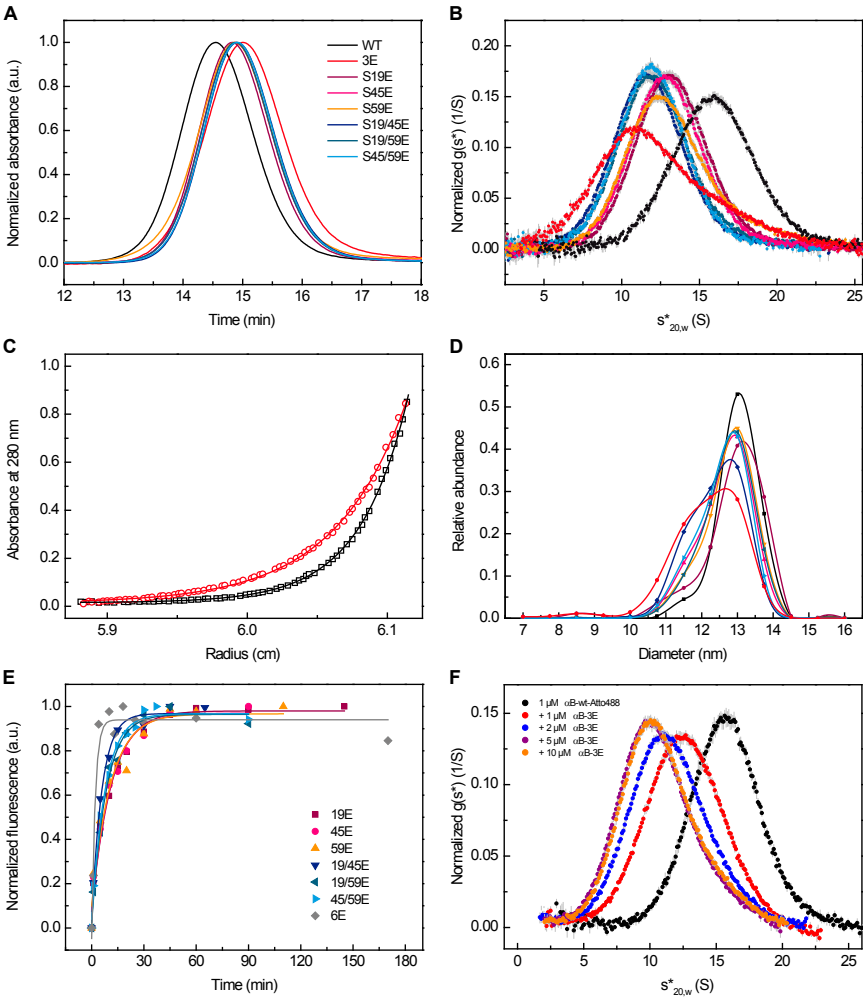

Fig. S2. Characterization of phosphorylation-mimetic mutants of αB. The quaternary structure of αB-WT and its single, double, and triple Glu mutants at the phosphorylation sites Ser19, Ser45, and Ser59 was analyzed by SEC (*A*), AUC (*B* and *C*), and negative-stain EM (*D*); oligomer dynamics were determined by subunit exchange FRET kinetics (*E*). The same color code was used throughout all panels: WT, black; 3E, red; 19E, purple; 45E, magenta; 59E, orange; 19/45E, blue; 19/59E, teal; 45/59E cyan. (*A*) SEC elution profiles of αB-WT and its phosphorylation-mimicking mutants. Data were collected using a Tosoh TSK 4000 PW column equilibrated in PBS. (*B*) Analysis of αB-WT and its phosphorylation-mimicking mutants by sedimentation velocity AUC (20 °C). Data analysis was carried out according to the dc/dt method; error bars are shown in light gray. Mimicking phosphorylation induces a shift to reduced $s_{20,w}$-values corresponding to smaller oligomers. (*C*) Concentration-radius plots obtained from sedimentation equilibrium AUC analysis of αB-WT (□) and αB-3E (○). The fit of the concentration distributions (straight lines) using a single exponential function yields average molecular masses of 490 kDa for αB-WT and 330 kDa for αB-3E. (*D*) Oligomer size distributions of αB-WT and its phosphorylation-mimicking mutants calculated from images of negatively stained samples using the largest (Feret) diameters (D_{max}) of the projection images as determined from corresponding class averages. (*E*) Subunit exchange kinetics of 1E, 2E, and 6E mutants of αB. Shown are the temporal changes in the donor fluorescence intensities at 415 nm due to reversal of FRET on adding excess amounts of the respective mutants to FRET-equilibrated hetero-oligomers of donor- and acceptor-labeled αB-WT-S153C (see Table S1 for calculated SX rate constants). (*F*) Fluorescence SV-AUC experiment to demonstrate the formation of WT/3E heterooligomers. The sedimentation of 1 μM Atto488-labeled αB-WT was selectively monitored with increasing amounts of unlabeled αB-3E. The size distribution of αB-WT is shifted toward smaller values on addition of αB-3E, indicating the formation of heterocomplexes with reduced average oligomer size. Instrument parameters and data analysis were the same as in *B*.

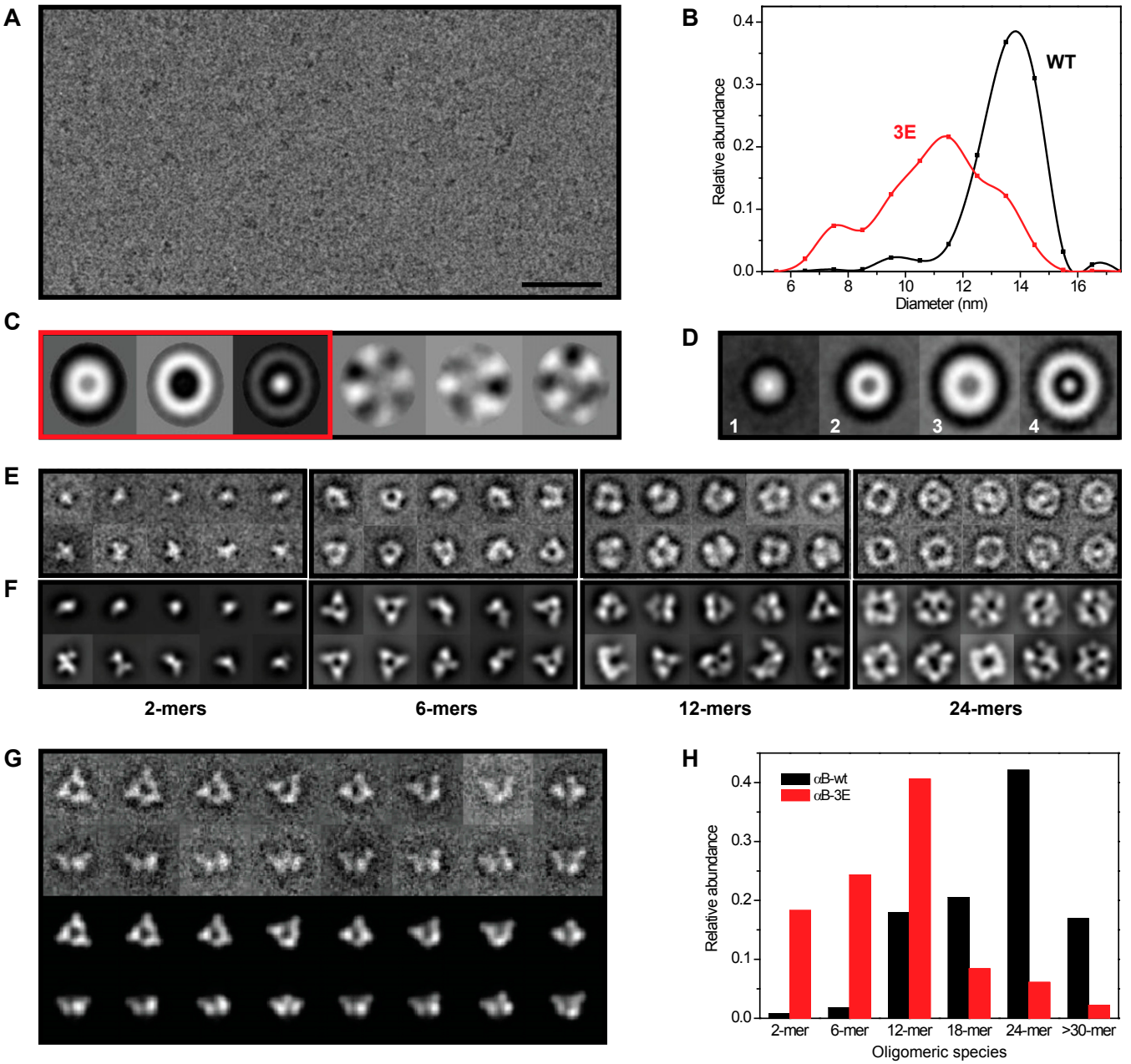

Fig. S3. Cryo-EM analysis of αB-3E. (*A*) Cryo-EM of αB-3E (0.2 mg/mL, pH 7.4). (Scale bar, 100 nm.) (*B*) Size distributions of the oligomers observed in cryo preparations of αB-WT (black) and αB-3E (red) calculated using the largest (Feret) diameters (D_{max}) of the projection images as determined from associated class averages. (*C*) First six eigenimages obtained after translational alignment of 24,424 projection images of αB-3E. (*D*) Class averages obtained on separation of the αB-3E data into four size populations (1–4) by MSA using the first three eigenimages (red box). Nineteen percent of the particles belong to class 1, 31% to class 2, 37% to class 3, and 13% to class 4. The diameters of the class averages are 6, 8, 11, and 13 nm, respectively. (*E*) Representative class averages of the populations 1–4 obtained on MSA without any further alignment and using the first 20 eigenimages for classification. (*F*) 2D reprojection images of the 3D models of αB 2-, 6-, 12-, and 24-mers derived from the pseudoatomic model of αB 24-mer (PDB 2YGD) obtained by cryo-EM (6). (*G*) Representative class averages (first and second rows) and corresponding reprojections of the reconstructed hexameric 3D volume (Fig. 2*A*) in the orientations found for the class averages (third and fourth rows). Box sizes (*C*–*G*): 18 nm. (*H*) Distribution of the main oligomer populations in αB-WT (black) and αB-3E (red).

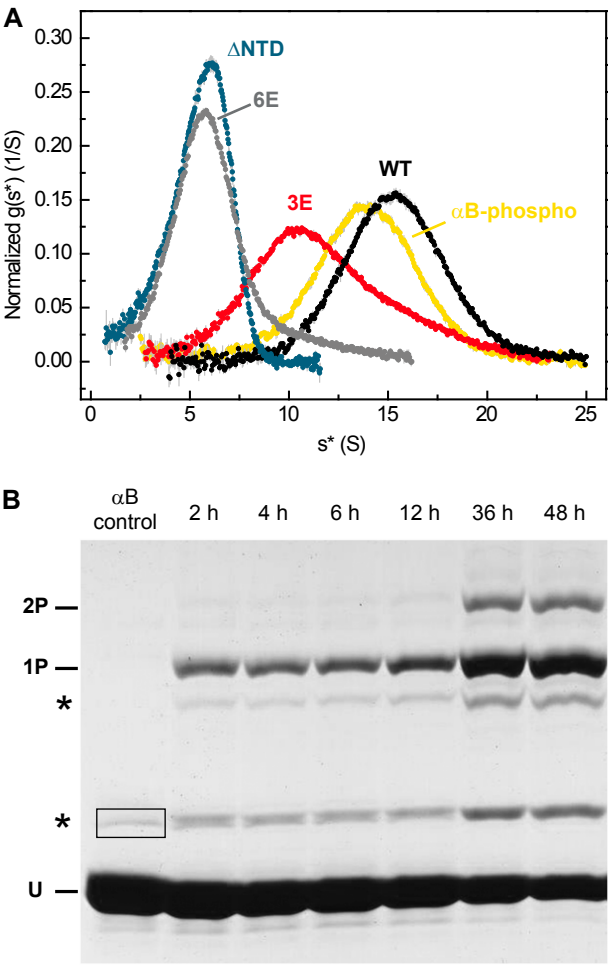

Fig. S4. Role of the NTD for oligomer formation. (*A*) Quaternary structure analysis of αB-6E (gray), αB-ΔNTD (teal), and αB-phospho (yellow) by sedimentation velocity AUC. Data collection and analysis were carried out as in Fig. S2*B*. αB-WT (black) and αB-3E (red) are depicted for comparison. (*B*) Phosphorylation of αB by MAPKAP kinase 2 was confirmed by electrophoresis using 12.5% Phos-tag gels. Aliquots were removed from the reaction at the indicated incubation times. The amount of unmodified (U) αB decreased over time, whereas new bands for single (1P) and double (2P) phosphorylated αB appeared. Additional bands (marked with an asterisk) could not be unambiguously assigned. However, these bands were identified as αB by MS analysis. The framed band of the αB control sample (without kinase) was unmodified, indicating an alternative conformation or assembly form the marked bands in the gel.

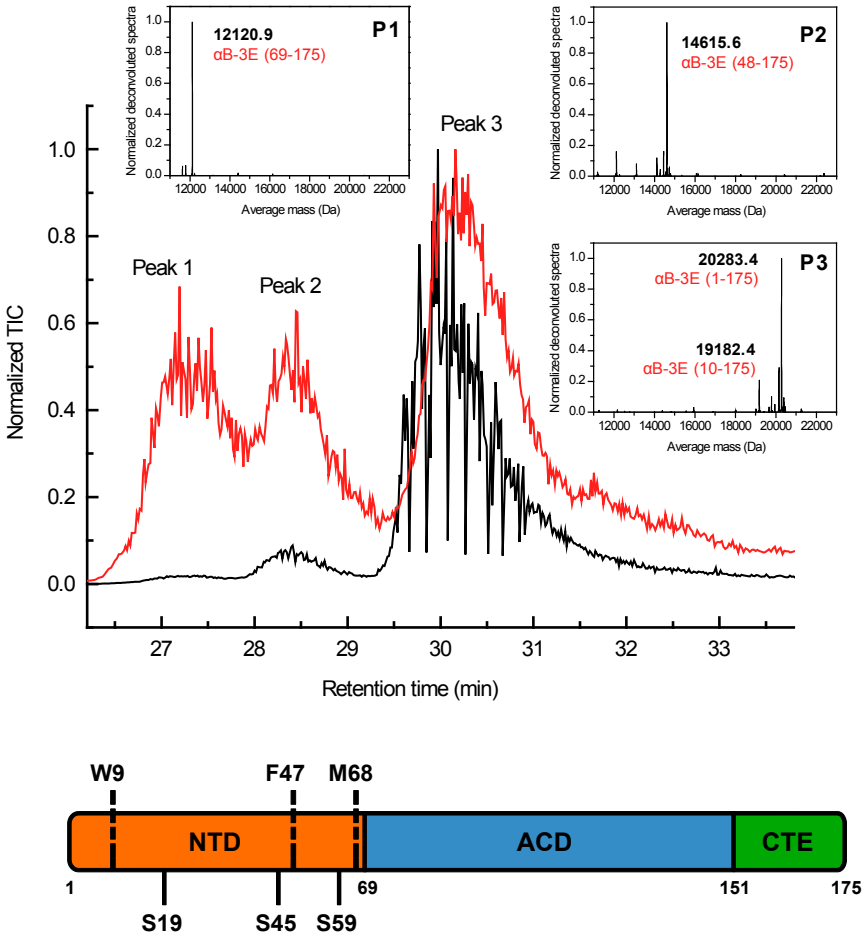

Fig. S5. Identification by LC-MS of the peptide products of proteolytic cleavage. Normalized total ion count (TIC) of partially digested αB-WT (black) and αB-3E (red) separated on a reversed phase column. Peaks 1–3 of the elution profile from αB-3E were averaged and deconvoluted using ProMass (Thermo Scientific). Resulting average masses 20,283.4, 19,182.4, 14,615.6, and 12,120.9 Da correspond to αB-3E full-length protein and protein cleavage before positions 10, 48, or 69, respectively. The cleavage sites are depicted in the domain organization of αB shown below.

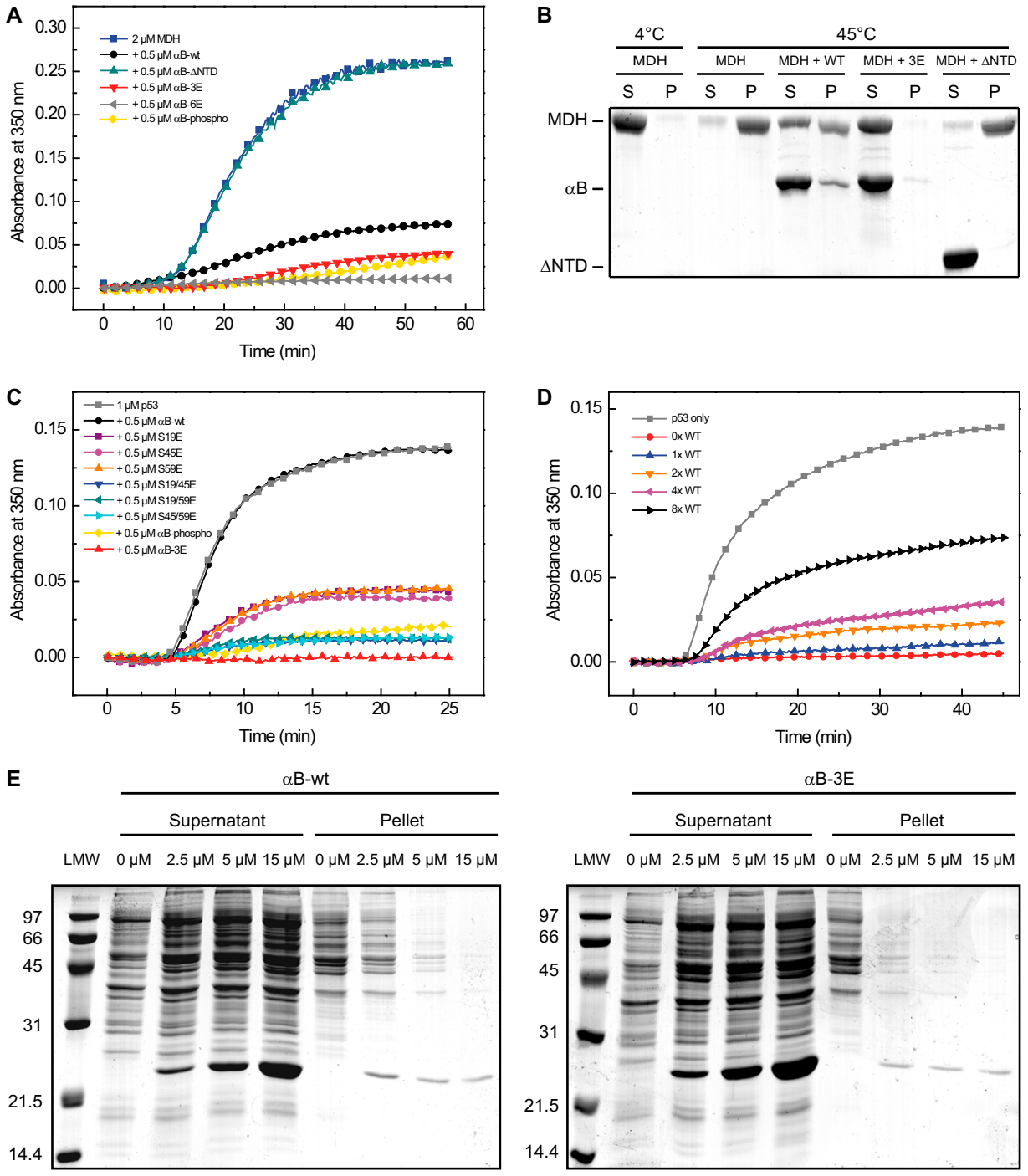

Fig. S6. Effects of mimicking phosphorylation on the chaperone function. (*A*) Aggregation of malate dehydrogenase (MDH). The aggregation reaction (2 μM MDH; blue squares) was induced by heat shock at 46 °C and monitored by absorbance at 350 nm. The chaperone activity of αB-WT (black), αB-3E (red), αB-ΔNTD (teal), αB-6E (gray), and αB-phospho (yellow) was assessed in the presence of 0.5 μM of the respective αB variant. (*B*) SDS/PAGE of the soluble [supernatant (S)] and insoluble [pellet (P)] fractions of MDH aggregation assays on separation by centrifugation (10 min, 10,000 × *g*). (*C*) Heat shock–induced aggregation of p53 at 42 °C (1 μM) monitored by absorbance at 350 nm in the absence (gray squares) and presence of 0.5 μM αB-WT, 1E, 2E, and 3E mutants. Coloring of the scattering curves is the same as in Fig. S2; αB-phospho is depicted in yellow. Note the intermediate activity of 1E and 2E mutants depending on the amount of introduced Glu residues. (*D*) Chaperone activity of αB-WT/αB-3E heterocomplexes at different ratios toward p53 (1 μM). The total concentration of αB-3E was kept constant at 0.5 μM. Note the decrease in chaperone activity with increasing amounts of αB-WT. (*E*) Aggregation suppression of heat-stressed HeLa cell lysate proteins. HeLa cell lysate (final absorbance $A_{280} \sim 2$) was heat-stressed at 45 °C for 40 min in the presence of various amounts of αB-WT (left gel) and αB-3E (right gel). The soluble [supernatant (S)] and the insoluble [pellet (P)] protein fractions were separated by centrifugation (10 min, 10,000 × *g*) followed by SDS/PAGE analysis. Both αB variants suppressed the aggregation of numerous lysate proteins, with αB-3E showing higher chaperone activity. Please note that both gels were run simultaneously and treated identically.

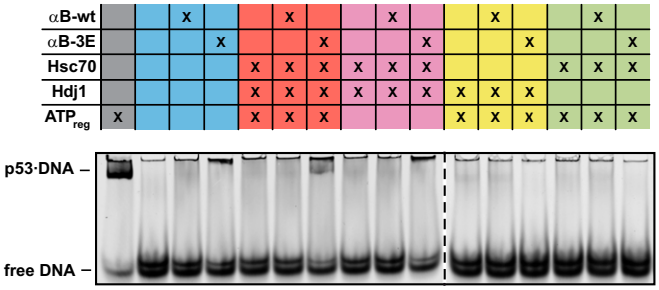

Fig. S7. Reactivation of heat-denatured human recombinant p53. The protein was denatured at 42 °C either without or in the presence of αB-WT and αB-3E. As a control, native p53 was kept at 4 °C (gray). Human Hsc70, Hdj1, an ATP regenerating system, αB-WT, and αB-3E were used in different combinations to rescue p53. To measure DNA-binding ability of reactivated p53, an EMSA with a specific Cy5-labeled DNA was performed. Note that the presence of αB-3E, Hsc70, Hdj1, and ATP is essential to yield reactivated p53 (red). Neither Hsc70 (yellow) nor Hdj1 (green) alone was sufficient. No reactivation was observed without ATP (violet). Please note that the image is composed of two separate gels (dashed line). Both gels were run and scanned simultaneously.

Table S1. Oligomer sizes (weight-average sedimentation coefficients) and subunit exchange rates of WT αB and its phospho-mimicking variants

αB variant	$<s_{20,w}>$ (S)	SX rate (min^{-1})
WT	16.19 ± 0.10	0.053 ± 0.013
S19E	13.34 ± 0.06	0.089 ± 0.009
S45E	13.13 ± 0.06	0.091 ± 0.012
S59E	13.47 ± 0.06	0.093 ± 0.017
S19/45E	11.96 ± 0.06	0.171 ± 0.017
S19/59E	12.29 ± 0.06	0.125 ± 0.022
S45/59E	12.04 ± 0.06	0.133 ± 0.015
3E (S19/45/59E)	12.29 ± 0.06	0.369 ± 0.028
6E (S19/21/43/45/53/59E)	6.31 ± 0.02	0.505 ± 0.132

Table S2. Dimensions and hydrodynamic parameters of αB-3E oligomers

Oligomer type	Molecular mass (kDa)	Dimensions of 3D reconstruction (nm)	R_g (nm)	Sedimentation coefficient (*S*)*
2-mer†	40	8.5 × 4.5 × 4.0 ± 1.5	2.9 ± 0.5	2.8 ± 0.25
6-mer (3 × 2)	121	11.0 × 11.0 × 6.0 ± 0.5	3.9 ± 0.1	6.0 ± 0.1
12-mer (2 × 6)	242	11.0 × 11.5 × 13.0 ± 0.75	4.8 ± 0.4	9.7 ± 0.4
24-mer (4 × 6)‡	485	13.5 × 13.5 × 13.5	5.8	16.1

R_g, radius of gyration obtained from hydrodynamic simulations.
*Svedberg obtained from hydrodynamic simulations.
†Average value calculated using the volumes occupied by the different 2-mers in the pseudoatomic model of αB 24-mer (PDB ID code 2YGD) (6) as input.
‡Calculated using the volume occupied by the 24-mer in the pseudoatomic model of αB 24-mer (PDB ID code 2YGD) (6) as input.

Other Supporting Information Files

Dataset S1 (XLSX)